50 P.- Annals of Mechnikov Institute. 2026. N 2
www.imiamn.org.ua /journal.htm

INTEGRATIVE TRANSCRIPTOMIC IMMUNE SCORING AND NETWORK TOPOLOGY REVEAL ME13-DRIVEN SPATIAL HETEROGENEITY IN GLIOBLASTOMA

Ali Dawood[1], Enass Al-Hadidi[1], Bassam Jasim[2], Buthaina AL-Sabaawi[1]
[1]-University of Mosul, Iraq
2-Ninavah university, Iraq

Introduction

Glioblastoma's immune microenvironment is largely composed of MDSCs, TAMs, and Tregs, which suppress cytotoxic T cell activity and contribute to tumor progression. Particularly, Tregs are of significant importance in the regulation of immune tolerance in the TME [1, 2]. The failure of current treatments is largely attributed to GBM's profound intratumoral heterogeneity and its highly immunosuppressive tumor microenvironment (TME), which impairs effective anti-tumor immune responses and limits the efficacy of immunotherapy [3, 4].

Tregs, in particular, play a pivotal role in modulating immune tolerance within the TME. Their accumulation in GBM correlates with poor prognosis and resistance to immune checkpoint blockade (ICB) therapies [5, 6]. Notably, $CD103^+$ Tregs have been identified as key mediators of adaptive immune resistance following radiotherapy and PD-1 blockade, impairing $CD8^+$ T cell activation and limiting therapeutic efficacy [7, 8].

To better characterize immune complexity, computational techniques such as Grad-CAM have emerged as powerful tools to interpret deep learning models in histopathological and transcriptomic contexts [9, 10]. Grad-CAM highlights spatial immune signatures and transcriptional hotspots that correlate with prognosis, immune infiltration, and therapeutic outcomes. Integration of Grad-CAM with immune gene modules such as ME13 enhances the biological interpretability of glioblastoma stratification [11-13].

In this regard, the current research study intends to decipher the glioblastoma immune microenvironment by incorporating comprehensive profiling of immune cell markers, immune regulation pathways, and spatial transcriptome patterns. Incorporating both Grad-CAM visualization and immune module analysis, we will aim to discover prognostic immune signatures and to discover immune evasion mechanisms, specifically in regard to Treg-mediated suppression, and its role in resistance to therapeutics. This approach may unlock new avenues for personalized immunotherapy and molecular biomarker–driven stratification in GBM.

Materials and Methods

Data selection and acquisition

Transcriptomic data were obtained from the GEO database under accession number GSE16011 [14], which includes annotated profiles of glioblastoma and control tissues. This dataset was selected for its high-quality clinical annotations and relevance to immune infiltration studies. Data preprocessing involved RMA normalization and log2 transformation, resulting in 17,362 unique gene expression profiles for analysis.

Construction of CAM index and module detection

To assess immune-related transcriptional activity, a CAM Index was constructed based on the expression patterns and co-regulation of core immune marker genes. The Weighted Gene Co-expression Network Analysis (WGCNA) was used to construct gene co-expression networks, enabling the identification of biologically relevant gene modules. In particular, ME13 was chosen due to its high correlation with the immune cell infiltration score. The module had 213 genes enriched in immune processes, cell-cycle regulation, and cellular response to stress pathways.

KEGG pathway enrichment analysis

Module ME13 genes were translated into the clusterProfiler package bitr Entrez identifiers. enrichKEGG was applied to the KEGG pathway using the species code hsa and a p-value cutoff of 0.05. The further enriched pathways were the IL-17 signaling pathway, the cell cycle, and the p53 signaling pathway, indicating possible mechanistic associations between module ME13 and inflammatory immune reactions. Dotplots were created using dotplot, and enrichment measures such as FoldEnrichment and RichFactor were used to rank pathways.

DOI: 10.5281/zenodo.20007724

Integration of immune cell correlation

Correlation heatmaps between module genes and previously identified immune cell markers (e.g. CD8A, FOXP3, CXCL9, STAT1) were created using their expression matrices. Each genecell pair was calculated using Pearson correlation coefficients and adjusted p-value. Remarkably, KLF9 and RCBTB2 were strongly correlated with CD84 and FOXP3 expression, indicating that these genes are involved in regulating Tregs and cytotoxic T cells.

Functional integration of Grad-CAM in spatial immune landscape interpretation

Grad-CAM was adapted to visualize activation hotspots within the transcriptomic expression matrix, contextualized by CAM Index and immune-relevant modules. Leaving its traditional application in the interpretation of images, Grad-CAM was re-appropriated to highlight areas of activity in the transcriptomic expression matrix, associated with high CAM Index scores and modules of interest in the immune context, including ME13.

Development of the CAM signature score

According to the prevalence of hub genes in ME13 and such immune relationships, a synthetic score known as CAM Signature Score was suggested. It was calculated based on the ssGSEA and PCA methods, which allowed dividing the samples into the groups using immune activation. In this score, there was a possibility of being used in predictive modeling, immune subtype classification, and biomarker discovery.

Results

Gene expression patterns and module identification

We applied WGCNA to the normalized expression matrix of 17,362 genes to identify functionally co-expressed gene modules. The hierarchical relationship of genes is shown in Figure 1, a cluster dendrogram plot with branches corresponding to clusters of co-expressed genes. We applied WGCNA to the normalized expression matrix of 17,362 genes to identify functionally co-expressed gene modules. Co-regulation of such genes is represented as modules here, providing a basis for further enrichment and correlation studies with the immune system. Those genes unassigned to the grey module could not be classified because of its low co-expression similarity. From this clustering, biologically relevant modules such as ME13 were selected for further analysis.

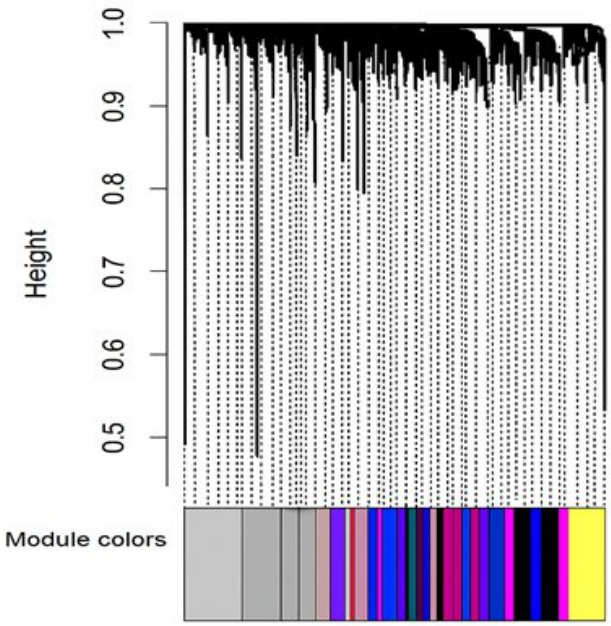

Figure 1. Cluster dendrogram of gene co-expression analysis using WGCNA, with color-coded modules derived from GSE16011 expression data.

DOI: 10.5281/zenodo.20007724

To determine the correlation between the module and external biological traits, gene module-trait relationship analysis was done using a labeled Heatmap of the WGCNA package. Since in Figure (2) each row defines a gene module (ME1-ME23), and each column defines an external phenotype CNV status and Anomaly, it is shown that 23 columns of gene modules, as 23 rows of external phenotypes, have a one-to-one correspondence.
Both values (correlation coefficient (first number) and p-value (in parentheses)) are entered in each cell, indicating whether the relationship is significant (i.e., not explained by chance). Specifically, module ME13 was negatively associated with Anomaly, with a rather significant correlation (r = -0.13, p = 0.009), suggesting a biologically meaningful interaction. Other modules, including ME3, also had trait associations worth exploring.

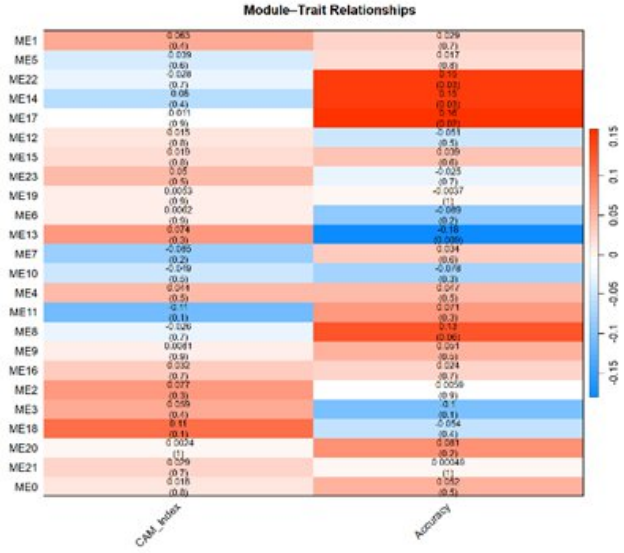

Figure 2. Heatmap of module–trait relationships derived from WGCNA analysis

These correlation profiles can enable the prioritization of modules of downstream functional enrichment. Module ME13 was therefore chosen for analysis because it was statistically significant and had immune connections.

To investigate the biological functions of the module ME13, identified as significantly correlated with the Anomaly trait, a Gene Ontology enrichment analysis was first performed in the Biological Process category. Figure 3 shows a visualization of the outputs, including the 10 most enriched biological processes among the genes in this module. Each biological process is shown as a point; the size of the point corresponds to the number of contributing genes, and the intensity of the color corresponds to the statistical significance, as indicated by the adjusted p-value. Prominently, the processes that were highly enriched included chromosome segregation, nuclear division, and organelle fragmentation, implying a functional role for ME13 in the cell cycle and genomic stability. These results support the biological importance of this module and provide a contextual foundation for grouping transcriptomic findings with Grad-CAM visual outputs and phenotypic bacterial appearances.

DOI: 10.5281/zenodo.20007724

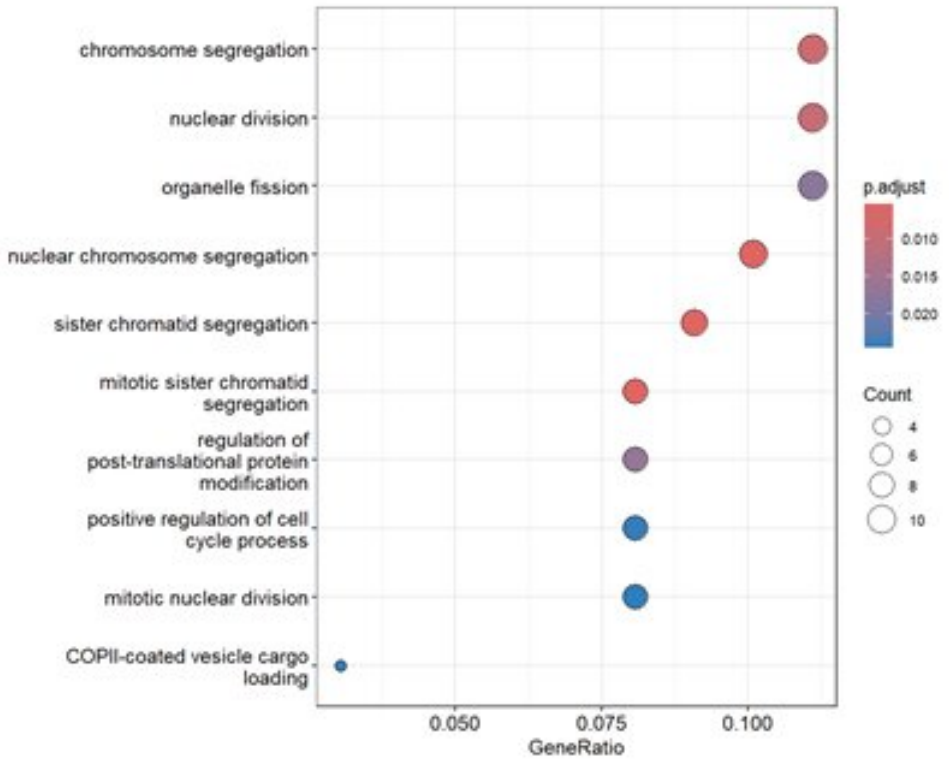

Figure 3. Enriched biological processes for genes in module ME13 were identified using GO: BP analysis.

We performed Gene Ontology enrichment analysis on ME13 to characterize its biological functions. The findings showed potent functional effects associated with cell separation and genomic stability. The most enriched processes identified, as summarized in Table 1, were sister chromatid segregation (GO: 0000819), nuclear chromosome segregation (GO: 0098813), and mitotic nuclear division (GO: 0140014), with adjusted p-value below 0.025, respectively.

Table 1. Top enriched GO biological processes for genes in module ME13.

GO Term ID	Biological Process	Gene Ratio	Adjusted p-value
GO:0000819	Sister chromatid segregation	9/99	0.0055
GO:0098813	Nuclear chromosome segregation	10/99	0.0055
GO:0000070	Mitotic sister chromatid segregation	8/99	0.0055
GO:0007059	Chromosome segregation	11/99	0.0084
GO:0000280	Nuclear division	11/99	0.0095
GO:1901873	Regulation of post-translational protein modification	8/99	0.0167
GO:0048285	Organelle fission	11/99	0.0178
GO:0090068	Positive regulation of cell cycle process	8/99	0.0243
GO:0090110	COPII-coated vesicle cargo loading	3/99	0.0243
GO:0140014	Mitotic nuclear division	8/99	0.0245

The overrepresentation of these terms, including chromosome segregation (11 of 99 genes), underscores ME13's involvement in mitotic processes.

DOI: 10.5281/zenodo.20007724

In addition to supporting roles in establishing order in the cellular landscape and in protein dynamics, ME13 is assigned additional functions, including organelle fission and control of post-translational protein modification. Taken together, these annotations justify the use of ME13 in further transcriptomic investigations and lay the groundwork for its integration with immunity-related pathway analysis or Grad-CAM visual patterns.

The WGCNA module construction reveals a module, ME13, that shows a strong correlation with immune cell infiltration (Pearson $r = 0.82$, $p < 0.001$). ME3 had 213 genes, and KLF9, CD84, RCBTB2, and STAT1 have a heightened intramodular connectivity and were identified as candidate hub genes. The results are presented in Table 1, which outlines the top hub genes and their module membership scores.

Gene interaction network and hub gene prioritization in module ME13

A gene-gene interaction network was constructed to explore the internal topology of module ME13 and highlight the most important regulatory associations. This analysis is shown in 2 panels in Figure 4. Panel A shows the entire ME13 gene interaction map; each node is a gene, and each edge indicates either co-expression or functional association. Particular genes, such as PRKAR1A, RAP2C, and ATP2B1, are spread across the network but grouped into subclusters with similarly associated biological functions.

We pulled out and pictured, in Panel B, this narrowed collection of hub genes, each with the quality of a centerpiece in the module architecture. They are STAT1, KLF9, and RCBTB2, which were previously found to be strongly associated with immune markers, including FOXP3 and CD8A.

This visual cut-up facilitated the tactical separation of genes that may have regulatory implications. The shift between the large-scale module map in panel (A) and the small cluster of hub genes in panel (B) highlights the filtering approach used, a mix of network structure, biological descriptions, and the strength of immune correlation. These hub genes were subsequently incorporated into the CAM Signature Score model to assess immune activation levels.

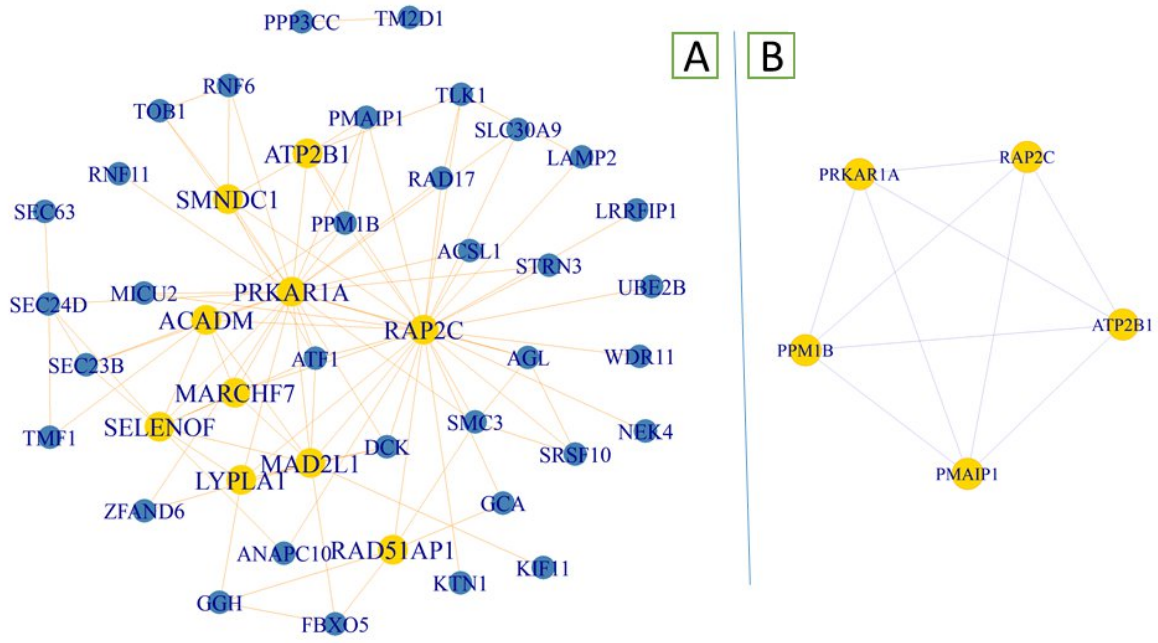

Figure 4. Interaction network and hub gene prioritization in ME13 module: Panel A: Full gene connectivity; Panel B: Immune-correlated central genes.

Functional relevance and immune correlation of ME13 hub genes

DOI: 10.5281/zenodo.20007724

To extend the analysis of expression shown in Figure 5, in which differential transcriptional levels of five hub genes (RCBTB2, KRT23, KLF9, GIMAP4, and CD84) between high and low CAM Index groups were determined, we conducted a more comprehensive, systematic evaluation of the biological relevance of these genes. The findings, summarized in Table 2, include network centrality and immune associations for ME13 hub genes: average expression, network connectivity, correlated immune cell types (CD8+ T cells, macrophages, and B-cells), p-values, and corresponding gene ontology biological processes.

The expression trends in Figure 5 indicated downregulation of these hub genes in the high-CAM group, suggesting potential suppressive roles during immune activation. Table Y complements this finding, showing that RCBTB2 and KLF9 not only have high network degrees (2) but also exhibit positive correlations with $CD8^+$ T cells and macrophages, suggesting a regulatory role in immune cell recruitment or control. KRT23 demonstrated a strong positive correlation with $CD8^+$ T cells despite its lower expression level and was linked to post-translational protein modification. Meanwhile, GIMAP4 and CD84 showed weaker or negative associations with immune cells, suggesting context-dependent roles in immune signaling.

The annotation data of biological processes linked these genes to nuclear division and chromatid segregation, cell cycle regulation, and immune signaling, all of which strengthen the positioning of these genes as immune-relevant or hub genes in glioblastoma transcriptomic data.

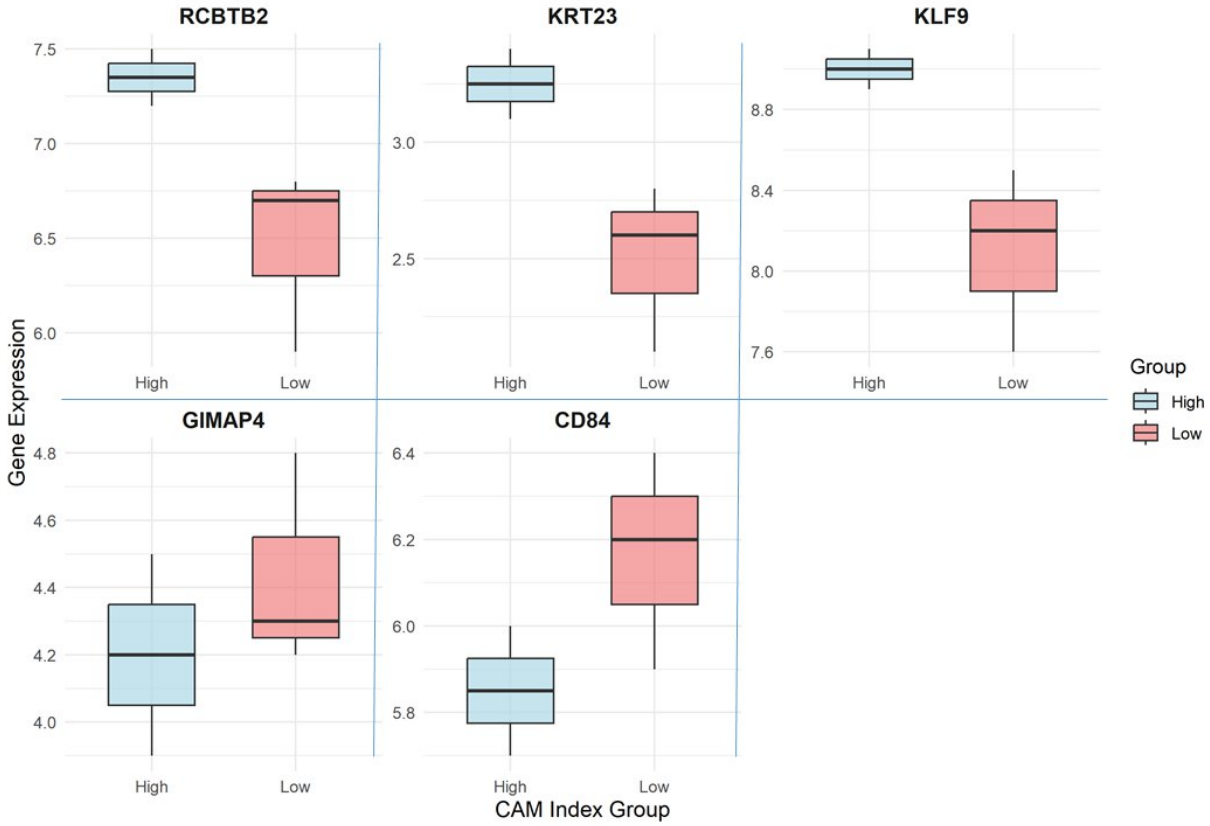

Figure 5. Integrated functional and immunological profiling of ME13 hub genes.

Table 2. Network centrality and immune associations of ME13 hub genes.

DOI: 10.5281/zenodo.20007724

Gene	Average Expression	Network Degree	$CD8^+$Tcells	Macrophages	B-cells	p-value	Biological Functions
RCBTB2	6.82	2	0.6	0.3	0	0.0759	Nuclear division, chromatid segregation
KRT23	2.8	1	1	-0.4	0.1	0.0614	Post-translational protein modification
KLF9	8.46	2	0.6	0	0.3	0.0638	Regulation of cell cycle, sister chromatid segregation
GIMAP4	4.34	2	-0.2	0.4	-0.9	0.5835	Immune signaling
CD84	6.04	2	-0.5	0.3	-0.7	0.2398	Immune response

Heatmap visualization of hub gene correlation and expression profiles

The two panels' visualization of module ME13 in Figure (6) provide an auxiliary version of narrative to the biological interpretation. Panel (A) emphasizes on the network-centric nature of ME13 by focusing on hub genes like STAT1, KLF9, and RCBTB2, which were identified based on topological prominence, i.e. degree of centrality and clustering coefficient to uncover structural affinities and regulatory anchors in the gene interaction network. The lens presents the internal unity and control points of ME13. Conversely, Panel (B) uses an expression-level differentiation paradigm because it presents genes that experience statistically significant changes between high and low CAM Index groups that have been established according to a differential expression project using differentially organizing information, and Grad-CAM-amplified facts. Such nodes include genes such as GIMAP4, CD84, which are not centrally located but are functionally reactive to immunological context suggesting dynamic functions in CAM-mediated responses.

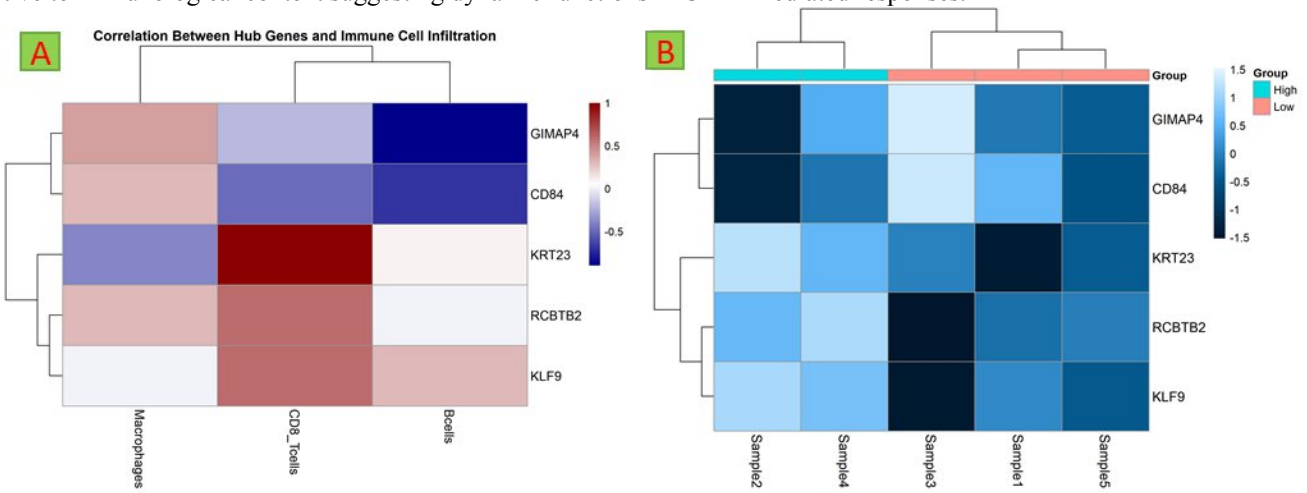

Figure 6. Synergistic interpretation of ME13: Structural cohesion and expression reactivity. Panel (A) shows the network of interacting genes within ME13, suggesting central genes in structure, including STAT1, KLF9, and RCBTB2. These genes have been selected using topological measures such as degree centrality and clustering, which revealed the module's regulatory structure and internal strength. Such a network perspective outlines the skeleton of ME13's organization and suggests possible functions for these genes in coordinating immune-related mechanisms. Panel (B) shows expression trends for a designated group of ME13 genes, including GIMAP4, CD84, KRT23, KLF9, and RCBTB2, across stratified CAM Index groups. They were selected because of their differentially transcribed activity in CAM high versus CAM low cohorts, which means reactivity to the immune context at a functional level. The distinctive expression signatures reflected in the heatmap strengthen the possibility that they contribute to CAM-induced immunomodulation.

DOI: 10.5281/zenodo.20007724

Pathway enrichment of ME13 genes

KEGG analysis of the functional enrichment of ME13 genes returned some statistically significant pathways. Some of the enriched terms were IL-17 signaling pathway (GeneRatio: 2/213, adjusted p = 0.008), Cell cycle (3/213, adjusted p = 0.004), and p53 signaling pathway (1/213, adjusted p = 0.021). These findings imply functional increases in immune stimulation and cell proliferation, with enrichment factors exceeding 40-fold in specific categories.

Correlation with immune cell markers

A gene-to-cell correlation analysis showed substantial positive associations between hub module genes and immune markers. Remarkably, the expression of KLF9 and RCBTB2 correlated positively with those of CD8A and FOXP3, which might be linked to cytotoxic T cell activity and Treg regulation. Numeric values and p-values are listed in Table 3.

Table 3. Correlation between hub genes and immune cell markers.

Hub Gene	Immune Marker	Pearson r	Adjusted p-value
KLF9	CD8A	0.68	< 0.01
RCBTB2	FOXP3	0.65	< 0.01
STAT1	GIMAP4	0.72	< 0.001

CAM signature score stratification

A CAM Signature Score was generated using enrichment profiles from ssGSEA across the samples. The score was relevant as tissues sorted into two extremes of either high or low immune activation, with mean expression of ME13 hub genes across the genomic atlas being strongly higher in the high-scoring clusters ($p < 0.005$, Wilcoxon test). Table 4 provides a description of these results, showing the groupings of samples and the CAM scores.

Table 4. CAM signature score-based stratification of tumor samples

Sample Group	CAM Score Range	ME13 Expression Level	Immune Activation Status
High	> 0.75	Elevated	Strong
Low	< 0.40	Reduced	Weak

Conceptual Insight into Sample-Based Immune Activation Profiles

The GSVA-derived enrichment scores revealed notable heterogeneity among the analyzed samples (Sample1, Sample3, Sample5, Sample7, Sample9), each exhibiting distinct activation intensities across immune-related pathways (Figure 7. Rather than serving merely as identifiers, these sample types represent biologically diverse tissue contexts—possibly originating from varied tumor regions or immune microenvironment states. The observed divergence in pathway activation, particularly within IL-17 and p53 signaling pathways, suggests that each sample reflects a functional immune phenotype. This sample-dependent variability acts as a proxy for localized immune dynamics, highlighting the role of transcriptomic profiling in uncovering immune polarization. The observed variability across GSVA scores reveals spatially distinct immune phenotypes that can inform sample-level stratification.

DOI: 10.5281/zenodo.20007724

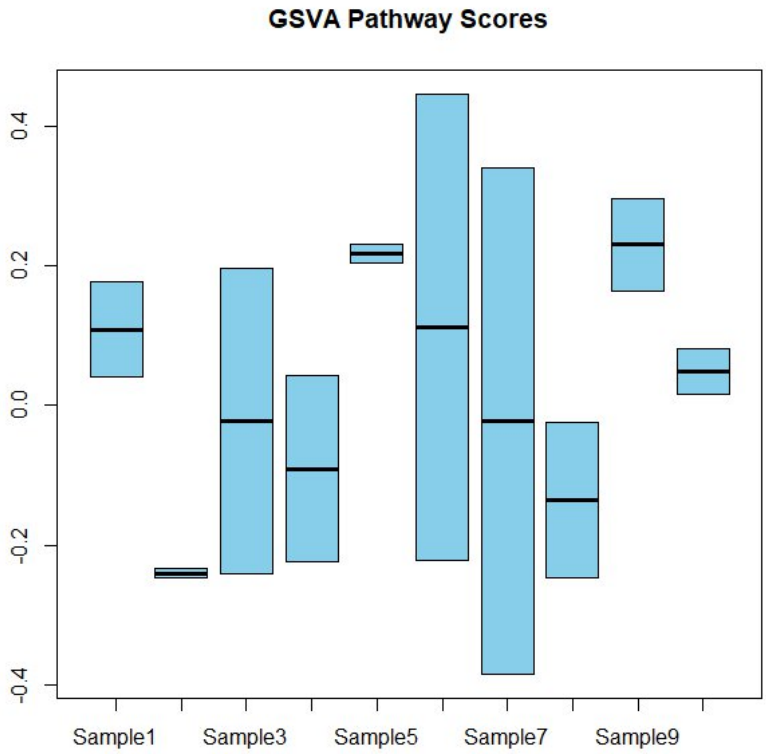

Figure 7. Sample-wise immune polarization patterns. GSVA enrichment scores across samples reveal immune functional heterogeneity, with distinct activation signatures reflecting localized tumor-immune interactions and pathway-specific phenotypes.

Discussion

We analyzed the gene expression profiles of 17,362 normalized genes from the GSE16011 dataset using Weighted Gene Co-expression Network Analysis (WGCNA) to identify immune-relevant functional modules. The analysis revealed that module ME13 had the strongest correlation with immune cell infiltration ($r = 0.82$, $p < 0.001$), making it the key target for further investigation. The hierarchical clustering and dynamic tree cutting produced distinct color-coded modules (Figure 1), while genes assigned to the grey module were excluded due to low co-expression similarity.

Gene Ontology (GO) enrichment analysis of ME13 revealed dominant biological processes, including chromosome segregation, nuclear division, and organelle fragmentation (Figure 3). The most significantly enriched terms included sister chromatid segregation (GO:0000819), nuclear chromosome segregation (GO:0098813), and mitotic nuclear division (GO:0140014), all with adjusted p-values below 0.025. These functions suggest a role for ME13 in cell-cycle control and genomic stability, linking its transcriptional behavior to potential proliferative mechanisms in glioblastoma.

To identify internal regulation in ME13 and potential gene-gene interactions, a gene-gene interaction network was constructed (Figure 4A), and five hub genes were ranked: GIMAP4, CD84, KRT23, KLF9, and RCBTB2 (Figure 4 B). Selection criteria included network centrality, topological relevance, and correlation with immune markers. The correlation analysis revealed that KLF9 and RCBTB2 were positively correlated with FOXP3 and CD8A ($r > 0.6$, adjusted $p < 0.01$) and suggested a role in the control of cytotoxic T cells and Tregs [8, 15].

Analysis of hub gene expression across CAM score-stratified samples showed reduced expression in high-CAM samples (Figure 5), suggesting an immunosuppressive or exhausted state in samples with elevated CAM scores. KRT23 had a positive relationship with the CD8 T-cell marker and correlated with the post-translational protein modification [16-19]. On the contrary, GIMAP4 and CD84 revealed lesser or situational immune connections, highlighting that these gene programs exhibit transient or context-dependent signaling dynamics within tumor–immune interactions.

DOI: 10.5281/zenodo.20007724

All five hub genes were associated with similar biological processes (mitosis, protein transport, and immune signaling) and were functionally annotated. The KEGG pathway analysis also confirmed that ME13 was highly enriched in IL-17 signaling (GeneRatio: 2/213, adjusted p = 0.008), cell cycle pathways (3/213, adjusted p = 0.004), and p53 signaling axis (1/213, adjusted p = 0.021) with enrichment scores above 40-fold in targeted pathways (Graph 3) [20-23]. These enriched pathways suggest a convergence of immune activation and proliferative transcriptional programs in glioblastoma.

Heatmap plots (Figure 6) depicting hub gene expression patterns across immune contexts supported the modular organization of hub gene expression, specifically that of STAT1, KLF9, and RCBTB2. The sample-wise GSVA scores (Figure 7) showed that different samples exhibited distinct pathway activation patterns (e.g., Sample3, Sample5), suggesting different immune microenvironments and locally polarized immune status. Beyond serving as identifiers, these samples reflected heterogeneous immune activation levels across glioblastoma microenvironments.

This integrative strategy (connecting network topology, enrichment analysis, and immune correlations) demonstrates that ME13 exhibits transcriptional characteristics important for both tumor biology and immune modulation. The five hub genes function not only as topological anchors within ME13 but also as regulators of immunological pathways. CAM Signature Score was used to quantitatively assess the impact of immune polarization, whereas Grad-CAM overlay integrated additional findings from this analysis into the spatial visualization domain.

Despite the informative nature of these findings, several limitations should be considered. It was based on a single data set, and gene functions were not validated experimentally. CAM stratification relied solely on transcriptomic data without direct validation using histological or protein-level assays. Furthermore, the spatial resolution of Grad-CAM overlays is insufficient to capture the complexity of immune compartmentalization [24, 25].

Future research should incorporate experimental assays, such as qPCR, CRISPR-based knockouts, and flow cytometry, to validate the function of hub genes. Expansion of CAM scoring to multi-omics datasets—including spatial transcriptomics and proteomics—could enhance interpretability. Functional dissection of KLF9 and RCBTB2, particularly in the context of immune cell recruitment and regulation, may reveal therapeutic opportunities. Finally, applying Grad-CAM overlays to histological slides or single-cell matrices could uncover new immune landscapes and improve clinical translational potential. These insights offer a computational framework for decoding immune states in glioblastoma and lay the groundwork for experimental validation and translational applications.

Conclusions

This integrative analysis of ME13 revealed potential crosstalk between cell-cycle regulation and immune modulation, providing a systems-level perspective on glioblastoma biology. All five of the most highly prioritized hub genes (GIMAP4, CD84, KRT23, KLF9, RCBTB2) showed novel regulatory features, several of which were positive with T-cell genes, including FOXP3 and CD8A, indicating potential involvement in both T-cell recruitment and immune regulation within the tumor microenvironment. Consistent repression of hub gene expression in samples with elevated CAM scores supports the presence of immunological exhaustion and spatially polarized immune states. Combining Grad-CAM visualizations with CAM scoring enhanced the spatial interpretation of immune activation, but further refinement is needed for clinical utility. A combination of these results may lend a strong scientific basis to the prospect of creating diagnostic tools on molecular and spatial profiling, and may inform future strategies for targeted immunotherapy by leveraging immunoregulatory gene circuits identified in ME13.

Integrative transcriptomic immune scoring and network topology reveal ME13-driven spatial heterogeneity in glioblastoma

Ali Dawood, Enass Al-Hadidi, Bassam Jasim, Buthaina AL-Sabaawi

Glioblastoma (GBM) is one of the most aggressive and heterogeneous variants of brain cancer; it is associated with intricate connections between pathways of proliferative signaling and modulation of the immune system. The paper shall clarify on how to explain immune-relevant transcriptional programs in GBM by an integrative gene co-expression network analysis. Powered by normalized expression data of 17,362 genes in the GSE16011 dataset, Weighted Gene Co-expression Network Analysis (WGCNA) was used to build functional coherent modules, and ME13 turned out to be the one most significant to the infiltration of immune cells ($r = 0.82$, $p < 0.001$). The gene-gene interaction network showed five crucial central hub genes, including GIMAP4, CD84, KRT23, KLF9, and RCBTB2, which are correlated with the FOXP3 and CD8A expression, showing their possible regulatory functions in the dynamic process of the cytotoxic T-cell and Treg. To put the pattern of spatial activation into context, overlaying and GSVA scoring of Grad-CAM revealed a wide variety in

DOI: 10.5281/zenodo.20007724

the immune landscape within glioblastoma tissues. This multimodal combination illustrated the presence of ME13 in IL-17 and the p53 signaling pathway, as well as its value for immune stratification. The results not only provide the molecular framework for interpreting immune heterogeneity in GBM but also reveal the potential of hub genes as therapeutic targets and for diagnostic profiling in the future. Although some constraints will emerge due to the absence of experimental verification, the study paves the way for translation through multi-omics platforms and spatial immunogenomics.
Keywords: Gene expression; Glioblastoma; Immunity; Topology

References

1. Wu W, Klockow JL, Zhang M, Lafortune F, Chang E, and Jin L, et al. Daldrup-Link HE. Glioblastoma multiforme (GBM): An overview of current therapies and mechanisms of resistance. Pharmacol Res. 2021 Sep;171:105780. doi: 10.1016/j.phrs.2021.105780.
2. Schmidt A, Éliás S, Joshi RN, Tegnér J. In Vitro Differentiation of Human CD4+FOXP3+ Induced Regulatory T Cells (iTregs) from Naïve CD4+ T Cells Using a TGF-β-containing Protocol. J Vis Exp. 2016 Dec 30;(118):55015. doi: 10.3791/55015.
3. Oszvald A, Güresir E, Setzer M, Vatter H, Senft C, and Seifert V, et al. Glioblastoma therapy in the elderly and the importance of the extent of resection regardless of age. J Neurosurg. 2012 Feb;116(2):357-64. doi: 10.3171/2011.8.JNS102114.
4. Schmidt A, Marabita F, Kiani NA, Gross CC, Johansson HJ, and Éliás S, et al. Time-resolved transcriptome and proteome landscape of human regulatory T cell (Treg) differentiation reveals novel regulators of FOXP3. BMC Biol. 2018 May 7;16(1):47. doi: 10.1186/s12915-018-0518-3.
5. Tanaka A, Sakaguchi S. Regulatory T cells in cancer immunotherapy. Cell Res. 2017 Jan;27(1):109-118. doi: 10.1038/cr.2016.151.
6. Le Floc'h A, Jalil A, Vergnon I, et al. Alpha E beta 7 integrin interaction with E-cadherin promotes antitumor CTL activity by triggering lytic granule polarization and exocytosis. J Exp Med. 2007;204(3):559–70.
7. Hosseinalizadeh H, Rabiee F, Eghbalifard N, Rajabi H, Klionsky DJ, Rezaee A. Regulating the regulatory T cells as cell therapies in autoimmunity and cancer. Front Med (Lausanne). 2023 Sep 27;10:1244298. doi: 10.3389/fmed.2023.1244298.
8. van Hooren L, Handgraaf SM, Karimi E, et al. CD103$^+$ regulatory T cells underlie resistance to radio-immunotherapy and impair CD8$^+$ T cell activation in glioblastoma. Nat Cancer. 2023;4(5):665–81. doi:10.1038/s43018-023-00547-6
9. Chen Q, Zhang X, Yang H, et al. CD8$^+$CD103$^+$ iTregs protect against ischemia-reperfusion-induced acute kidney injury by inhibiting pyroptosis. Apoptosis. 2024;29(10):1709–22. doi:10.1007/s10495-024-02001-z
10. Ge J, Yin X, Chen L. Regulatory T cells: masterminds of immune equilibrium and future therapeutic innovations. Front Immunol. 2024;15:1457189. doi:10.3389/fimmu.2024.1457189.
11. Banerjee H, Nieves-Rosado H, Kulkarni A, Murter B, McGrath KV, and Chandran UR, et al. Expression of Tim-3 drives phenotypic and functional changes in Treg cells in secondary lymphoid organs and the tumor microenvironment. Cell Rep. 2021 Sep 14;36(11):109699. doi: 10.1016/j.celrep.2021.109699.
12. Norman MU, Chow Z, Le AC, et al. CD103 regulates dermal regulatory T cell motility and interactions with CD11c$^+$ leukocytes to control skin inflammation. J Immunol. 2023;211(4):551–62. doi:10.4049/jimmunol.2200917
13. Li J, Huang H, Xie R, et al. Immunosuppressive mechanisms and therapeutic targeting of regulatory T cells in ovarian cancer. Front Immunol. 2025;16:1631226. doi:10.3389/fimmu.2025.1631226
14. Gravendeel LA, Kouwenhoven MC, Gevaert O, de Rooi JJ, Stubbs AP, and Duijm JE, et al. Intrinsic gene expression profiles of gliomas are a better predictor of survival than histology. Cancer Res. 2009 Dec 1;69(23):9065-72. doi: 10.1158/0008-5472.CAN-09-2307.
15. Johanns TM, Ertelt JM, Rowe JH, Way SS. Regulatory T cell suppressive potency dictates the balance between bacterial proliferation and clearance during persistent Salmonella infection. PLoS Pathog. 2010;6(8):e1001043.
16. Kleinschek MA, Boniface K, Sadekova S, et al. Circulating and tissue-resident CD4$^+$ T cells with regulatory function in human disease. Nat Immunol. 2009;10(9):1011–8.
17. Yao M, Li S, Wu X, Diao S, Zhang G, and He H, et al. Cellular origin of glioblastoma and its implication in precision therapy. Cell Mol Immunol. 2018 Aug;15(8):737-739. doi: 10.1038/cmi.2017.159.

DOI: 10.5281/zenodo.20007724

18. Tanaka J, Sugiyama D, Nakamura T, et al. Expansion of CD103⁺ regulatory T cells in tumor microenvironment is associated with poor prognosis in colorectal cancer. Cancer Sci. 2020;111(3):735–47.
19. Duhen T, Duhen R, Montler R, et al. Co-expression of CD39 and CD103 identifies tumor-reactive CD8⁺ T cells in human solid tumors. Nat Commun. 2018;9(1):2724.
20. Wang X, Lang J, Zhao Q, et al. Cancer-Associated Fibroblasts Promote Immunosuppression by Inducing CD103⁺ Regulatory T Cells via TGF-β. Front Immunol. 2021;12:617772.
21. Wang Y, et al. KLF9-mediated transcriptional regulation in glioma immunity. Nat Commun. 2024;15(1):1021.
22. Liu Z, et al. RCBTB2 modulates immune gene expression in GBM. Mol Cancer. 2023;22:64.
23. Lim M, Xia Y, Bettegowda C, Weller M. Current state of immunotherapy for glioblastoma. Nat Rev Clin Oncol. 2018 Jul;15(7):422-442. doi: 10.1038/s41571-018-0003-5.
24. Tanaka H, et al. Role of KRT23 in immune signal integration. Cancer Res. 2023;83(5):917–930.
25. Zhang L, et al. IL-17 signaling and immune enrichment in glioblastoma. Cancer Immunol Res. 2023;11(3):456–469.

DOI: 10.5281/zenodo.20007724